Validation of Simulation Capability for RF Wave Propagation and Absorption in the Ion Cyclotron Range of Frequencies on Alcator C-Mod*

P. T. Bonoli 1), A. Bader 1), N. Tsujii 1), R. W. Harvey 2), E. F. Jaeger 3), D. B. Batchelor 4), L. A. Berry 4), Y. Lin 1), R. Parker 1), M. Porkolab 1), J. C. Wright 1), S. J. Wukitch 1), and the Alcator C-Mod Team.
1) Plasma Science and Fusion Center, MIT, Cambridge, MA, (USA).
2) CompX, Del Mar, CA 92014 (USA).
3) Xcel Engineering, Oak Ridge, TN 37830 (USA).
4) Oak Ridge National Laboratory, Oak Ridge, TN 37830 (USA).

Email: bonoli@psfc.mit.edu

Abstract: Radio-frequency (RF) heating experiments have been performed in the Alcator C-Mod tokamak that utilize the minority heating scheme in the ion cyclotron range of frequencies (ICRF). These experiments were performed in deuterium majority and hydrogen minority plasmas at $B_0 = 5.4$ T, $I_p = 0.6 – 1.0$ MA, $n_e(0) \approx 1 - 2 \times 10^{20}$ m^{-3}, with $n_H / n_e \approx 4$-8%, an ICRF source frequency of 80 MHz and at a power level of 2 – 4 MW. A compact neutral particle analyzer (CNPA) was used to detect neutralized fast ions associated with the ICRF generated minority hydrogen tail and those measurements were used to test a simulation capability for ICRF minority heating that combines a full-wave electromagnetic field solver and a zero ion orbit width Fokker Planck code. Non-thermal ion tails simulated with this combined model were used in a synthetic diagnostic code for the CNPA and preliminary comparisons with the measured signals were made for discharges at high current (1 MA) and low current (0.6 MA). Finally we have begun to benchmark a reduced model for ICRF wave propagation valid in the ion Finite Larmor radius (FLR) regime against a more complete wave propagation code valid to all orders in ($\rho_i / \lambda_\perp$).

1. Introduction

Radio-frequency power in the ion cyclotron range of frequencies (ICRF) is primarily used on the Alcator C-Mod tokamak for plasma heating via the fundamental (minority) ion cyclotron resonance heating scheme [1]. Furthermore, mode converted ion Bernstein waves (IBW) and ion cyclotron waves (ICW) have been shown on C-Mod to be effective for sawtooth modification ("pacing") [2] via localized current profile modification and more recently for generation of toroidal plasma rotation [3]. In order to interpret and optimize these applications of ICRF power on Alcator as well as on other present day devices and ITER [4] we have undertaken to verify and validate a predictive simulation capability for the propagation, absorption, and mode conversion of ICRF waves. One of the outstanding challenges in performing these simulations arises from the multiple spatial scales that exist when fast magnetosonic waves mode convert to much shorter wavelength electrostatic ion Bernstein waves (IBW) or electromagnetic ion cyclotron waves (ICW). Even in the minority heating regime where power flow to the mode converted wave branch is small, it is nonetheless important to simulate both modes correctly in order to have an accurate estimate of the fast wave polarization in the resonance layer. Furthermore, RF waves interact in a highly nonlinear fashion with thermal and nonthermal particles in the plasma. This occurs because nonthermal ion distributions are produced by the ICRF wave as it damps strongly on a dilute minority ion population. Recently a Compact Neutral Particle Analyzer (CNPA) with expanded measurement capability in space and energy (relative to its predecessor [5]) was installed on Alcator C-Mod. This diagnostic has been used to infer the energy distribution of an ICRF-generated minority hydrogen tail in C-Mod by detecting neutralized fast ions associated with the energetic minority tail charge exchanging with background ions in the plasma. Those measurements have been used to test a model for ICRF heating [6] that combines a full-wave ICRF solver and a zero ion orbit width Fokker Planck code. The

technique used for validation is to reconstruct the CNPA signal in a synthetic diagnostic code using the nonthermal ion distribution simulated by the full-wave / Fokker Planck model.

As the minority hydrogen or ^{3}He concentrations are increased in deuterium majority plasmas in C-Mod, a transition is seen to the so-called mode conversion electron heating regime [7, 8]. In these discharges a phase contrast imaging (PCI) diagnostic has been used to detect mode converted ICW and IBW [7, 8]. In the present work we describe results in which a reduced model for ICRF wave propagation valid in the ion Finite Larmor radius (FLR) regime has been benchmarked against a more complete wave propagation code valid to all orders in (ρ_i / $\lambda_\perp$) using a series of discharges with increasing minority ion concentration in C-Mod. We also describe calculations to accurately study the transition from minority heating to mode conversion by using a combined full-wave / Fokker Planck model, so as to properly account for the effect of the energetic minority tail in the transition regime to mode conversion.

2. Compact Neutral Particle Analyzer Diagnostic

The CNPA is a diagnostic that measures the fast neutral flux exiting the plasma. The data in this paper are collected from five HS1-20 electrically biased silicon-diode detectors located on top of the tokamak, ~3.2 m above the plasma midplane. The detectors are covered with a 150 nm foil that prevents visible light from contaminating the signal. Incoming particles create charge-hole pairs in the semi-conductor in proportion to their energies. The processing electronics are similar to a precurser CNPA operated on C-Mod [5] with the notable exception that energy resolution has been sacrificed to extend the energy range to 2 MeV. The CNPA detectors and electronics were calibrated between 500 keV and 1.1 MeV using a particle accelerator and show excellent linearity in that range.

The CNPA has proven to be a robust tool to measure the fast-ion population produced by ICRF minority heating on C-Mod. Charge exchange processes are the main methods of fast ion neutralization and impart a negligible change in particle momentum or energy. Thus measuring an escaping fast neutral provides information on the energy and phase angle of the ion at the time of its neutralization. The CNPA sightlines are shown in *FIG. 1*. The detectors view through an adjustable aperture plane located ~2.5 m above the plasma midplane, one aperture for each detector. Each CNPA detector has two sightlines, a straight down view and a diagonal view that looks through the aperture of the adjacent detector. All other views are cut off by the walls of the vertical port. The inner three channels have diagonal views that view the outer edge of the plasma. The diagonal views for the three inner channels have negligible impact on the total CNPA signal. The outer two channels have diagonal views that view back towards the resonance layer. These views have considerable impact on the CNPA signal. Another notable difference between the present diagnostic set-up and that used in the past [5]

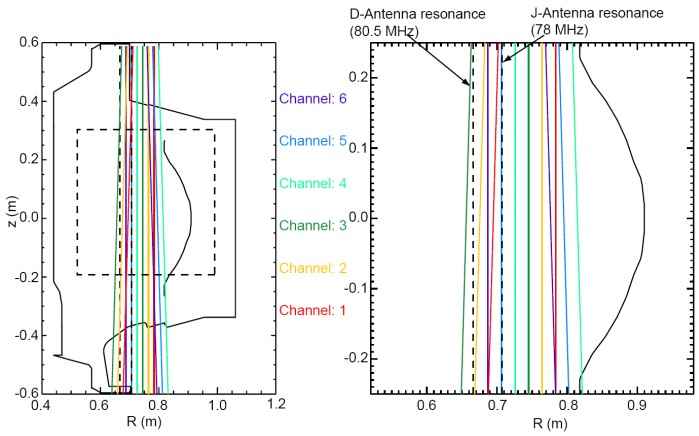

FIG. 1: Left panel: The six CNPA sightlines shown in the Alcator C-Mod cross-section. Right panel: Blow-up of sightline paths with minority hydrogen resonance layers (B_0 = 5.3 T) overlaid for reference.

is that the diagnostic sightlines now cover major radii from R = (68 – 78) cm, whereas previously the range was from R = (66 – 70) cm.

3. Description of simulation models and synthetic diagnostic

3.1 Simulation Models

Wave fields in the minority absorption scenario are simulated using two full-wave electromagnetic solvers. Both codes consider a rapidly oscillating wave field **E** with frequency ω, in which case Maxwell's equations reduce to the Helmholtz wave equation:

$$-\nabla\times\nabla\times\mathbf{E}+\frac{\omega^2}{c^2}\left(\mathbf{E}+\frac{i}{\omega\varepsilon_0}\mathbf{J}_p\right)=-i\omega\mu_0\mathbf{J}_{ant} \qquad (1)$$

where the plasma current $\mathbf{J}_p$ is, in general, a non-local, nonlinear, integral operator on the electric field. The first code that is used is the All Orders Spectral Algorithm AORSA [9] which is spectral in all three dimensions (R, Z, ϕ). Here (R, Z, ϕ) are cylindrical coordinates where 'R' lies in the equatorial plane of the tokamak, 'Z' is the vertical dimension, and 'ϕ' is the toroidal angle. The code includes all cyclotron harmonics in the evaluation of the plasma conductivity and no assumption is made about the perpendicular wavelength ($\lambda_\perp$) relative to the ion gyroradius (ρ_i). The plasma response formulated in this manner leads to an integral relation and the resulting matrices that must be inverted are large, dense, non-symmetric, indefinite, and complex [9]. A second field solver TORIC [10, 11] is also used which employs a mixed spectral, finite element representation for the electric field in (ρ, θ, ϕ), where (ρ, θ, ϕ) are the usual pseudo-toroidal coordinates. The conductivity relation is truncated at first order in $(\lambda_\perp / \rho_i)^2$ and at the second cyclotron harmonic. These assumptions result in a closed form for the plasma response and a matrix system to invert that is sparse and banded with large dense blocks.

A self-consistent simulation of ICRF heating requires a description of the wave propagation and absorption in the plasma as well as the quasilinear response of the plasma to the wave heating. The long time scale response of the plasma distribution function f_0 is obtained from the bounce-averaged, zero ion orbit width Fokker-Planck code CQL3D [12] which solves an equation of the form:

$$\frac{\partial}{\partial t}(\lambda f_0)=\nabla_{\boldsymbol{u}_0}\cdot\Gamma_{\boldsymbol{u}_0} \quad \text{with } \nabla_{\boldsymbol{u}_0}\cdot\Gamma_{\boldsymbol{u}_0}=C(f_0)+Q(\mathbf{E},f_0). \qquad (2)$$

In these expressions: $\boldsymbol{u}_0$ is the velocity vector at the outside midplane; $\lambda = \tau_b u_{\|0}$, with bounce time τ_b; and C and Q are, respectively, the bounce-averaged collision and quasilinear operators. This is a nonlinear problem in which the energetic ions generated by the waves can significantly alter the wave propagation and absorption in the plasma. To obtain self-consistency AORSA and CQL3D are iteratively coupled [13]. The plasma response in AORSA is evaluated [14] using the most recent numerical non-thermal ion distribution function from CQL3D. The new RF wave fields from AORSA are then used to evaluate an RF diffusion coefficient which is used to further evolve the ion distribution in the Fokker Planck code. In the present work only the steady state solution of Eq. (2) is solved for at each iteration with the full-wave solver.

3.2 Synthetic diagnostic code for the CNPA

A synthetic diagnostic was created for the CQL3D code to simulate the neutral flux to a detector located outside of the plasma. The neutral flux to the detector can be written as [15]:

$$\frac{\partial n}{\partial t} = \int_0^{S_{plasma}} ds\, I(s,E)\, A(s,E), \qquad (3)$$

where (∂n / ∂t) is given in units of [particles /(sec × cm^2 × steradians ×eV)], E is the neutral energy, "s" is the integration distance along a specified viewing chord from the detector located at the plasma edge to a distance S_{plasma}, where the sightline leaves the plasma, *I(s, E)* is the neutral density emittance in units of [particle # / (sec × cm^2 × steradian × eV)], and *A(s, E)* is the attenuation of emitted neutrals, for example by re-ionization. The neutral density emittance can be written as [15]:

$$I(s,E_0,\Omega_0) = \int d^3u'\, f_b(u') \int d^3u\, f_a(u) \int d\Omega\ \sigma_{CX}\ \delta(E-E_0)\ \delta(\Omega-\Omega_0)\left|v-v'\right|, \qquad (4)$$

where f_b is the distribution function of neutral atoms, f_a is the fast ion (minority) distribution function computed by CQL3D, σ_{CX} is the charge exchange cross-section, and Ω_0 refers to the solid angle for scattering in the direction of the detector. Therefore, to determine the neutral flux the density distributions of the neutrals and relevant impurity species (in our case B^{4+}) are needed. Also the cross sections for neutralization and ionization reactions must be determined. The density of background deuterium (D^0) is obtained from the TRANSP code, where the D^0 density at a given flux surface is the sum of neutrals transported from the cold plasma at the wall and neutrals that arise through recombination reactions in the plasma. The B^{4+} density is calculated solely from coronal equilibrium considerations [16], where transport from the wall is not considered for the boron. The B^{5+} density is estimated at 1% of n_e [17] for Alcator C-Mod plasmas.

Charge exchange cross-sections are also needed for the synthetic diagnostic. Cross sections for the reaction $H^+ + D^0 \Rightarrow H^0 + D^+$ are not available, but do not differ significantly from cross-sections for reactions $H^+ + H^0 \Rightarrow H^0 + H^+$. Cross sections for these reactions are available for fast proton energies up to 10 MeV [18]. Cross sections for $H^+ + B^{4+} \Rightarrow H^0 + B^{5+}$ are available from theoretical calculations up to 600 keV [19]. Above 600 keV, cross-sections are unavailable. However, theoretical calculations are available for $H^+ + C^{5+} \Rightarrow H^0 + C^{6+}$ up to 2 MeV [20] and the theoretical cross sections from carbon were used to estimate the shape of the curve for high energy charge exchange with boron.

4.0 Experimental results from the CNPA and comparisons with simulation

An example of an ICRF heated discharge where CNPA data was collected is shown in *FIG. 2*. The hydrogen minority absorption scheme was used with plasma parameters B_0 = 5.4 T, I_p = 1.0 MA, and $\overline{n}_e \approx 1 - 1.3 \times 10^{20}$ m^{-3}. The ICRF source power was provided by three antennas that were driven at 80.5 MHz, 80.0 MHz, and 78.0 MHz. The ICRF pulse was modulated with a 40 msec on time and a 40 msec off time in order to eventually study the time dynamics of the fast minority tail. The minority hydrogen concentration in this discharge varied between $n_H / n_e \approx$ 4-8%. The signature of an energetic minority ion tail being created by the ICRF power and then slowing down via electron drag is evident in the central electron temperature which increases from about 2 to 4 keV during each ICRF pulse. The CNPA counts versus time are also plotted in *FIG. 2* for four of the six viewing channels shown in

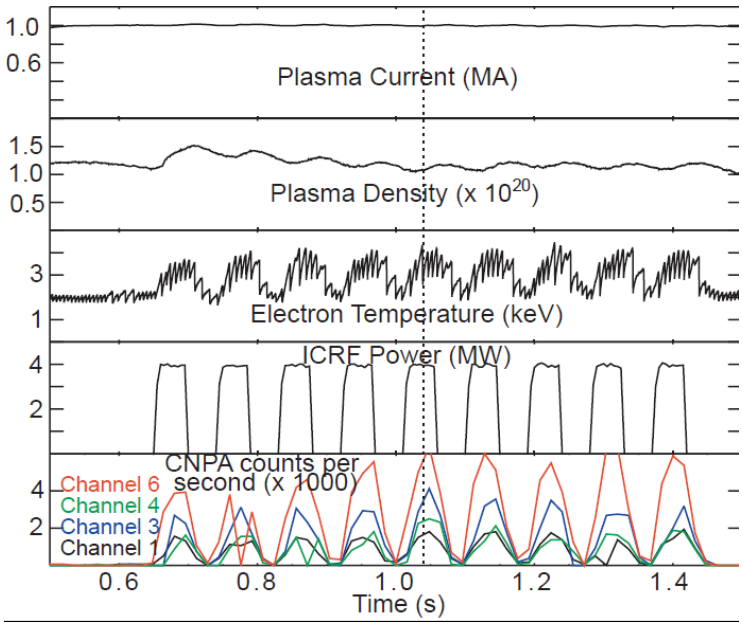

FIG. 2: Plasma discharge in Alcator C-Mod with ICRF minority heating where CNPA data was collected through an ICRF power modulation technique. Plasma density is line average measurement and electron temperature is peak value.

FIG. 1. Interestingly, the CNPA signal can be seen to persist beyond the turn-off time for each ICRF pulse as the fast ion tail decays via collisional slowing down.

FIGURE 3 displays one of the main results of this paper which is a comparison of the measured and simulated CNPA energy spectra for four of the sightlines, taken at a time corresponding to the dashed line in *FIG. 2*. The simulated signals were obtained from an AORSA – CQL3D simulation using a single ICRF frequency of 80 MHz, a single toroidal mode number of $n_\phi = 10$, $P_{ICRF} = 4$ MW, $n_H / n_e = 5\%$, and a spectral resolution of 128 (k_X) × 128 (k_Y) modes. AORSA and CQL3D were iterated four times to achieve convergence. The simulated spectra qualitatively reproduce the energy dependence of the measured spectra in that they continue to drop off (by an order of magnitude) at higher energies (≈ 1 MeV). Also the magnitude of the simulated spectra agree quantitatively with the measured values for CNPA channels 2-4. The disagreement seen in the simulated and measured values for the

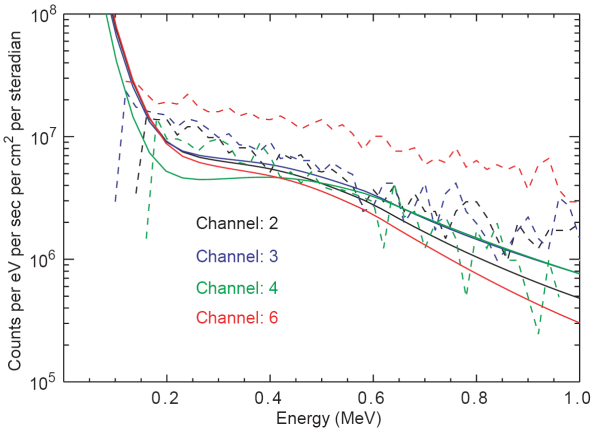

FIG. 3: Comparison of the measured (dashed lines) and simulated (solid lines) CNPA energy spectra for CNPA channels 2,3,4, and 6 at the time of 1.025 sec (see FIG. 2).

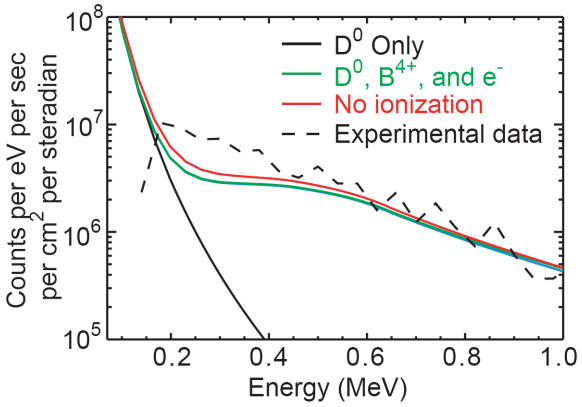

FIG. 4: Comparison of measured and simulated CNPA spectra for channel 4 showing the effect of including charge exchange due to background boron versus only background D^0.

innermost channel [see channel 6 on *FIG. 1*] is not understood at this time but will be investigated in future studies. It is important to note that absolute magnitudes have been plotted for the simulated spectra. Another important finding is shown in *FIG. 4* where the measured CNPA signal for a single channel is compared with the simulated signal assuming the fast minority ion tail charge exchanges only with background D^0 versus both D^0 and B^{4+}. It can be clearly seen that charge exchange with the background B^{4+} must be accounted for in order to reproduce the measured CNPA signal. Removing the electron recombination showed

no significant difference in the simulated signal. The converged power density ($\partial W / \partial t$) from the full-wave / Fokker Planck iteration corresponding to *FIG. 3* is shown in *FIG 5*, where it can be seen that most of the 4MW of injected ICRF power is damped on the minority hydrogen tail (≈ 3.75 MW), as would be expected. The remaining power is damped at the second harmonic deuterium cyclotron resonance layer (≈ 0.5 MW). Direct electron absorption of the fast wave is negligible in this case (≈ 0.05 MW).

Finally we show in *FIG. 6* a comparison of the measured and simulated CNPA signals for a low current (0.6 MA) discharge in C-Mod at B_0= 5.4T, with 3 MW of ICRF minority heating, again delivered by three antennas operating at 80.5 MHz, 80.0 MHz, and 78.0 MHz. The ICRF pulse was modulated with a 40 msec on time and off time and the plasma density was

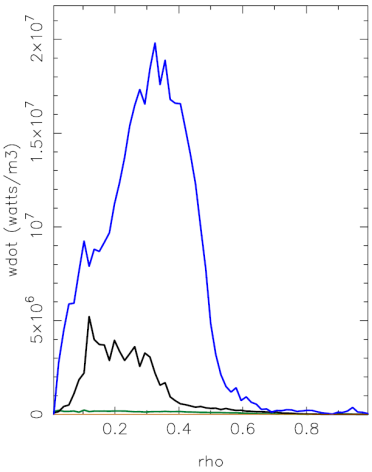

FIG. 5: ICRF power density ("wdot") versus normalized radius ("rho") for the AORSA-CQL3Dsimulation. The blue, black, and green curves correspond respectively to minority hydrogen absorption, second harmonic deuterium absorption, and direct fast wave electron absorption.

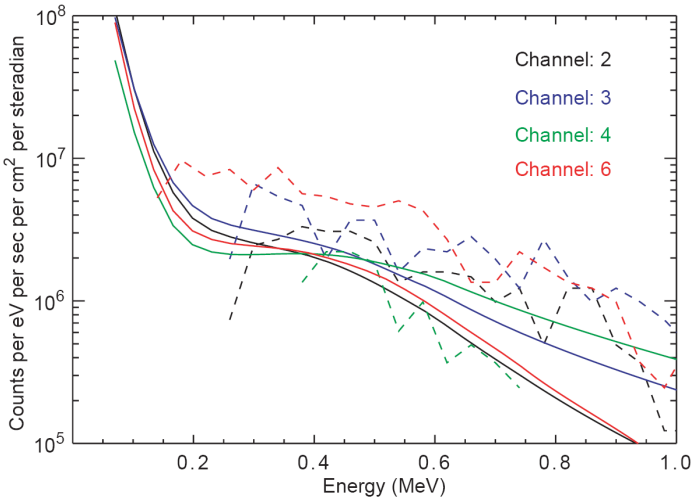

FIG. 6: Comparison of the measured (dashed lines) and simulated (solid lines) CNPA energy spectra for CNPA channels 2,3,4, and 6 for an 0.6 MA discharge in C-Mod with 3 MW of ICRF minority heating.

In the range $\overline{n}_e \approx 1 - 1.3 \times 10^{20}$ m^{-3}. The simulated spectra exhibit the same energy dependence as the measured spectra, dropping significantly at higher energy and again the measured spectra on channel 6 is significantly higher than the simulated values. However there is not the agreement in magnitude of the measured and simulated spectra for channels 2, 3, and 4 that was found in the 1.0 MA case (see *FIG. 3*). Since finite ion orbit losses are not included in the AORSA-CQL3D modeling this disagreement in magnitude might possibly be attributed to that deficiency in the modeling. However only channel 4 fits that explanation where the simulated value is *higher* than the measured value.

5. Benchmarking of the AORSA and TORIC full-wave solvers

In Section 3.1 it was pointed out that although the ICRF physics in the AORSA solver is more complete, the computational requirements to obtain converged solutions are significantly greater than in a "reduced physics" model such as the TORIC solver. We have thus started to benchmark TORIC against AORSA in order to determine under what conditions the physics

kernel in TORIC is valid. Results for two such benchmark studies are shown in *FIGS. 7-8*. In *FIG. 7* the hydrogen minority fraction was scanned and in *FIG. 8* the ^{3}He minority fraction

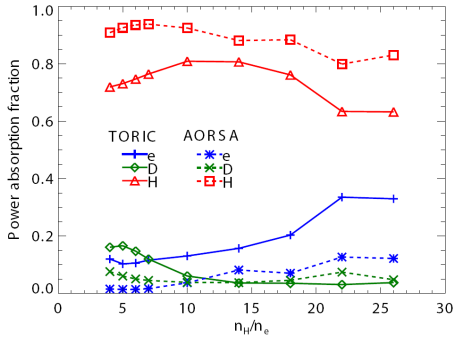

FIG. 7: Benchmark results for TORIC and AORSA solvers using Alcator C-Mod parameters for a hydrogen minority concentration scan.

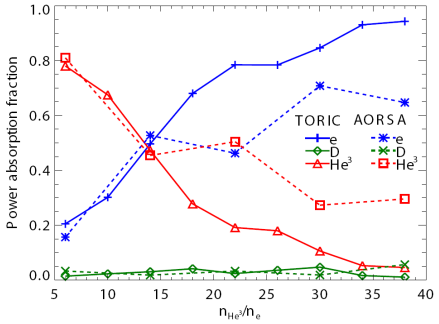

FIG. 8: Benchmark results for TORIC and AORSA solvers using Alcator C-Mod parameters for a ^{3}He minority concentration scan.

was varied and in each scan the minority ion component was assumed to remain thermal. The parameters used in the hydrogen scan were [$B_0 = 5.4$ T, $I_p = 0.9$ MA, $n_e(0) = 1.8 \times 10^{20}$ m^{-3}, $T_e(0) = 1.8$ keV, $f_0 = 80$ MHz, and $n_\phi = 10$, for $n_H / n_e < 10\%$] and [$B_0 = 6$ T, $I_p = 0.8$ MA, $n_e(0) = 1.5 \times 10^{20}$ m^{-3}, $T_e(0) = 2.8$ keV, for $n_H / n_e \geq 14\%$]. The parameters used in the ^{3}He scan were [$B_0 = 8$ T, $I_p = 1.2$ MA, $n_e(0) = 1.2 \times 10^{20}$ m^{-3}, $T_e(0) = 5.0$ keV, $f_0 = 78$ MHz, and $n_\phi = 7$]. These scans reveal two unexpected results. First in the hydrogen minority scan at $n_H / n_e < 10\%$ (see *FIG. 7*) the code predictions differ more than what would be expected since the ion FLR approximation used in TORIC should be very good in that regime. Conversely the codes agree very well in the ^{3}He minority scan at $n_{He\text{-}3}/ n_e < 14\%$ where the ion FLR approximation used in TORIC might start to beak down. In both scans however, the basic trends predicted by AORSA and TORIC for absorption on ions and electrons are qualitatively

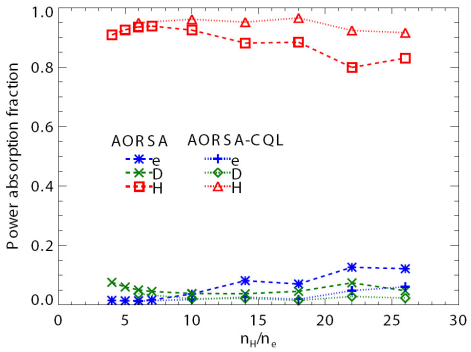

FIG. 9: Results for the AORSA and AORSA-CQL3D hydrogen minority concentration scan using Alcator C-Mod parameters.

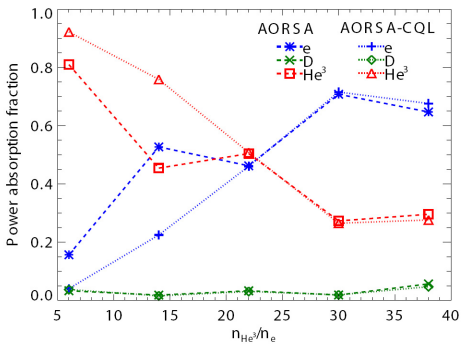

FIG. 10: Results for the AORSA and AORSA-CQL3D ^{3}He minority concentration scan using Alcator C-Mod parameters.

the same. Finally in order to elucidate the role of quasilinear tail formation on the transition from the minority heating to mode conversion electron heating regime we have repeated the AORSA scans in *FIGS. 7-8* with the coupled AORSA-CQL3D model (see *FIGS. 9-10)*. In both the (H) and (^{3}He) scans the effect of the quasilinear tail is to increase the minority absorption relative to what are predicted using thermal ions only. This effect is especially pronounced in the ^{3}He scan (see *FIG. 10*) and points to the importance of including the quasilinear tail formation when studying the transition from minority heating to the mode conversion regime.

6. Summary

First results from a Compact Neutral Particle Analyzer (CNPA) have been compared with a combined full-wave / Fokker Planck model (AORSA / CQL3D) for hydrogen minority heating in Alcator C-Mod. Simulated fast ion distributions were used in a synthetic diagnostic code for the CNPA and preliminary comparisons with experiment are encouraging, especially at high current where energetic ions are well-confined. The simulated spectra qualitatively reproduce the energy dependence of the measured spectra and the magnitude of the signal is comparable to experiment without renormalization of the data. In the near future we plan to use AORSA and CQL3D iteratively in time in order to study the time dynamics of minority ion tail formation and decay. This work will be greatly facilitated by using a computational framework [21] from which AORSA and CQL3D can be initiated automatically in a changing background plasma. We also presented results in which the reduced model TORIC solver was compared against the more complete AORSA code. Although quantitative differences in RF absorption were found as minority concentration was scanned, both codes were found to exhibit the same qualitative trends with increasing minority concentration. Finally a concentration scan with the combined AORSA-CQL3D code demonstrated the importance of including the effect of quasilinear tail formation when studying the transition to mode conversion.

*Work supported by the United States Department of Energy.

[1] BONOLI, P. T., et al., Fusion Science and Technology **51**, (2007) 401.
[2] WUKITCH, S. J., et al., Physics of Plasmas **12**, (2005) 056104.
[3] LIN, Y., et al., Physics of Plasmas **16**, 056102 (2009).
[4] GORMEZANO, C., et al., Nuclear Fusion **47**, (2007) S285-S336.
[5] TANG, V., et al., Plasma Physics and Controlled Fusion **49**, (2007) 873.
[6] JAEGER, E. F., et al., Nuclear Fusion **46**, (2006) S397.
[7] NELSON-MELBY, E., et al., Physical Review Letters **90**, (2004) 155004.
[8] LIN, Y., et al., Plasma Physics and Controlled Fusion **47**, (2005) 1207.
[9] JAEGER, E. F., et al., Physics of Plasmas **9**, (2002) 1873.
[10] BRAMBILLA, M., Plasma Physics and Controlled Fusion **41**, (1999) 1.
[11] WRIGHT, J. C., et al., Physics of Plasmas **11**, (2004) 2473.
[12] HARVEY, R. W. and McCoy, M., "The CQL3D Fokker Planck Code," Proc. IAEA Tech. Comm. Meeting on Simulation and Modeling of Thermonuclear Plasmas, Montreal (1992).
[13] JAEGER, E. F., et al., Nuclear Fusion **46**, (2006) S397.
[14] DUMONT, R. J., PHILLPS, C. K., and SMITHE, D. N., Physics of Plasmas **12**, (2005) 042508.
[15] HARVEY, R. W., "X-Ray Energy Spectra Calculated from CQL3D Fokker-Planck Electron Distributions", Report CompX-2000-2 (2000).
[16] The ADAS Project: Atomic Data and Analysis Structure: http://open.adas.ac.uk.
[17] MCDERMOTT, R. M., et al., Physics of Plasmas **16**, (2009) 056103.
[18] JANEV, R. K., and SMITH, J. J., "Atomic and Plasma-Material Interaction Data for Fusion" (IAEA, Vienna, 1993) Vol. 4.
[19] WINTER, T. G., Physical Review A **56**, (1997) 2903.
[20] WINTER, T. G., Physical Review A **69**, (2004) 042711.
[21] ELWASIF, W. R., et al., in Proceedings of the 18th Euromicro International Conference on Parallel, Distributed and Network-Based Computing, 2010, Pisa, Italy.